The influence of bottom morphology on far field reflectance: theory and 2-D model.

J.Ronald V.Zaneveld and Emmanuel Boss

College of Oceanic and Atmospheric Sciences

Oregon State University

Corresponding author address:

Emmanuel Boss

College of Ocean and Atmospheric Sciences,

Oregon State University

Corvallis, Or, 97331

boss@oce.orst.edu

ABSTRACT

The reflectance of the bottom is of importance when interpreting optical data in shallow water. Closure studies of radiative transfer, interpretation of laser line scanner data, lidar, and remote sensing in shallow waters require understanding of the bottom reflectance. In the Coastal Benthic Optical Properties experiment (CoBOP), extensive measurements of the material reflectance (reflectance very close to the bottom) were made. In carrying out closure of the radiative transfer model and observed radiometric and Inherent Optical Properties, what will be needed however is the far field reflectance. The far field reflectance is the bottom reflectance that includes the effect of bottom morphology (such as sand ripples) as well as the material reflectance. We present here a first order analytical model to derive the relationship between the material and far field reflectances. We show that the effective reflectance of the bottom is proportional to the average cosine of the bottom slope. Using a simple 2-dimensional geometry without scattering and absorption we show that errors in ignoring the bottom morphology can lead to overestimations of the far field reflectance on the order of 30%.

INTRODUCTION

Shallow water optical signals are influenced by the bottom reflectivity. Closure of radiative transfer calculations, determination of the contrast of objects with the bottom such as measured by laser line scanners, inversion of remotely sensed radiance for bathymetry, and diver visibility can all be improved with proper knowledge of the bottom reflectance. Many bottoms are nearly Lambertian surfaces, surfaces for which the detected radiance is independent of the viewing angle (Mobley,1994). The radiance reflected from a bottom is not independent of the irradiance on the bottom, however. Therefore, a bottom with topography has a reflectance that is different from a flat, horizontal bottom. Bottom reflectances are usually measured on scales of cm (Voss, 1999). We call this the material reflectance, although it includes small scale morphology such as individual grain size. Larger scale morphology is not included in direct measurements of the bottom reflectance. Radiance and irradiance detectors at larger distances from the bottom will thus see the effect of bottom morphology.

The reflectance of surfaces is a function of both the incident light direction and the emitted light direction. This is the bidirectional reflectance distribution function (BRDF, Voss, 1999). For surfaces where the BRDF is strongly asymmetric it is obvious that changing the relative incident and emitted light directions, by tilting the bottom, will have a strong effect. Many bottoms, such as sand, are nearly Lambertian, however (Mobley,1994). In that case the radiance $L(\theta)$ emanating from the bottom in any direction θ is given by $L(\theta) = \rho\ E_b /\pi$, where ρ is the material reflectance of the bottom and E_b is the irradiance at the bottom (measured parallel to the bottom). In the simplest case, the incoming light is collimated and vertical and has a downwelling irradiance E. The irradiance impinging on the bottom is then $E_b = E \cos(\theta_b)$, where E_b is the irradiance at the bottom and θ_b is the angle of the bottom with the horizontal. Changing the angle of incidence of the incoming light will also change the irradiance and hence the radiance emanating from the bottom. Even in the simplest case it is then seen that the radiance emanating from the bottom depends on all factors that determine the irradiance at the bottom. These factors include the incoming radiance distribution (which in turn is determined by the radiance distribution just above the sea surface, the sea surface, and the IOP of the water column), the morphology of the bottom, and the geometries of the radiance detector and light source. The theoretical model derived here shows that all these factors are potentially important.

It is the far field reflectance (or effective reflectance) that must be used in radiative transfer calculations in the case of the detector footprint being larger than the bottom roughness scale. For example, in its experimental design the closure studies of the Coastal Benthic Optical Properties (CoBOP) program did not consider bottom morphology. It is thus worthwhile evaluating the magnitude of the bottom morphology on plane parallel radiative transfer calculations such as used in CoBOP. Similarly, remote sensing observations that are used to infer bathymetry must also take this into account.

Allen's (1982) monumental review contains ample information on bottom morphology and the associated slopes. The steepest bed forms are associated with wave ripples and underwater dunes which, on average, have ratios of wavelength to height of about 5. Bottom ripples occur anytime a current moves over a bed of sand, silt, or clay. The specific morphology produced depends on the nature of the bottom and the strength, direction, and duration of the water movement. Wave ripples were the characteristic bedform in the sand flats adjacent to the fringe reefs on the Exuma side of LSI. In contrast, Adderley Cut and Rainbow South were characterized by large shallow underwater dunes. In the former case a radiance sensor's field of view would cover many ripples, whereas in the latter case, the sensor would likely cover one side of an underwater dune only. Both these cases will be analyzed in this paper.

THEORY

We will briefly review the definition of radiance in order to set the stage for the subsequent development of the dependence of the far field reflectance on the morphology of the ocean bottom. Figure 1 shows the general geometry of a source and detector system. It is well known (for example Jerlov, 1976) that the radiance is reciprocal, i.e. the radiance from the source to the detector is the same as the radiance from the detector to the source.

We derive here the reflectance observed by a finite radiance detector due to a multi-faceted bottom. Secondary reflections of the light by the bottom are ignored. Light attenuation is also ignored in order to isolate the effect of bottom morphology and hence to derive an effective reflectance that can be used in models in lieu of the usual

Lambertian reflectance. Light absorption and scattering can be added in radiative transfer models that can include the sea surface by using the MTF approach as in Zaneveld et al. (2001).

In the following discussion the bottom is considered to be the light source as daylight is reflected from it. The radiant flux between a source and a detector is given by Φ . Units are W. The angles θ_d and θ_s are relative to the line connecting the centers of the source and detection areas. This line need not be perpendicular to the sea surface, as both the detector and the bottom may be tilted relative to the vertical. (See also Jerlov, 1976, for a good description of the fundamental relationships of radiance.)

The source radiance L is defined by the radiant flux per unit solid angle per unit projected area of surface. Units are W/m^2 ster .

The solid angle of the detector is defined as:

$$\Omega_d = A_s \cos\theta_s / r^2. \qquad (1)$$

The projected area of the detector perpendicular to the line joining the centers of the source and the detector is $A_d \cos\theta_d$

The radiance of the source is thus:

$$L = \frac{\Phi r^2}{A_d \cos\theta_d \, A_s \cos\theta_s} \quad \text{for } A_d \ 0;\ A_s \ 0, \qquad (2)$$

Note the symmetry in the expression for the radiance. If we interchange the source and detector the expression is the same.

If the source is Lambertian, the radiance in any direction is :

$L = \rho E_s/\pi$, where ρ is the reflectance of the source (bottom) and E_s is the irradiance at the source (bottom).

We assume that the incoming light is collimated and just below the surface has a solar zenith angle of θ_z. If the collimated irradiance measured perpendicular to the direction of propagation of the photons is E, the irradiance at the bottom, E_s , is:

$$E_s = E \cos|\theta_z - \theta_b|, \tag{3a}$$

where θ_b is the angle of the bottom with the horizon in the plane of the incoming light. Note that θ_b need not be equal to θ_s as the line connecting source and detector need not be perpendicular to the sea surface. The absolute value of the difference of the zenith angle and the bottom angle is required as the irradiance is always positive.

The general case requires knowledge of the radiance distribution at the bottom.

The irradiance parallel to the bottom in the general case is given by:

$$E_s(x,y,b) = \int_0^{2\pi} \int_0^{\pi/2} L(\theta,\phi,x,y,b) \cos|\theta - \theta_b(x,y)| \sin\theta \, d\theta \, d\phi. \qquad (3b)$$

The irradiance at some point (x,y,b) on the bottom thus depends on the local radiance $L(\theta,\phi,x,y,b)$, as well as the local angle of the bottom with the horizon, $\theta_b(x,y)$. For clarity, we will continue our discussion for the collimated radiance case only, although the above expression for E_s for the general case may always be substituted in the equations.

The radiance of the source to the detector in the collimated radiance case is:

$$L = \rho E \cos|\theta_z - \theta_b| / \pi, \qquad (4a)$$

which by definition is the same as the radiance due to the source perceived at the detector. It is clear that the radiance of the source (bottom) depends on the cosine of the angle of the bottom with the vertical. Note that the radiance does not depend on the solid angle or area of the detector. Eq.4 is the radiance that would be detected in the case of a simple sloping bottom, such as the side of a large underwater sand dune. We then have an effective reflectance equal to :

$$\rho_{eff} = \rho \cos|\theta_z - \theta_b|. \qquad (4b)$$

The radiant flux received by the detector as obtained from Eq.2 and substituting Eq.4 is:

$$\Phi = \frac{L\ A_d \cos\theta_d\ A_s \cos\theta_s}{r^2} = \frac{\rho\ E \cos|\theta_z - \theta_b|\ \ A_d \cos\theta_d\ A_s \cos\theta_s}{\pi\ r^2}\ . \qquad (5)$$

In practice a radiance detector is not infinitely small. It therefore has a finite detector area and a finite solid angle of detection. This results in the radiance detector averaging the radiance from an area of the bottom, where the bottom may not be flat. What is this average radiance?

Such a realistic radiance detector's detection solid angle might well simultaneously see several source areas with different slopes θ_s. We approximate the bottom as consisting of a number of facets each with a constant slope angle. Properties such as described in the previous section, but for an individual facet, have the added subscript i. The radiant flux from one small source area i within the larger detected area to the detector would then be:

$$\Phi_i = \ L_i\ \Omega_{di}\ A_d \cos\theta_{di} \qquad (6)$$

Each individual area would have a radiance L_i and a detection solid angle $\Omega_{d\,i}$, and a normal detection area $A_d \cos\theta_d$. The local radiance would be:

$$L_i = \rho\ E \cos|\theta_z - \theta_{bi}|\ \ /\pi. \qquad (7)$$

Only fluxes from the facets to the detector can be added linearly. Radiance cannot be added linearly, since the solid angles subtended by the facets need not be the same in the general case. The solid angle of detection for the small area i, Ω_{di} , is given by:

$$\Omega_{di} = A_{si}\cos\theta_{si} / r_i^2. \qquad (8)$$

The radiant flux (Watts) received at the detector from the small area i is then:

$$\Phi_i = \frac{\rho\, E \cos|\theta_z - \theta_{bi}|\ \ A_{si}\cos\theta_{si}\ A_d\cos\theta_{di}}{\pi\, r_i^2}\ . \qquad (9)$$

Note the parallel between Eqs. 9 and 5. The total flux received by the detector is then:

$$\Phi_{total} = \sum_i \frac{\rho\, E \cos|\theta_z - \theta_{bi}|\ \ A_{si}\cos\theta_{si}\ A_d\cos\theta_{di}}{\pi\, r_i^2}\ . \qquad (10)$$

The radiance perceived by the finite detector is the total radiant flux divided by the solid angle and detector surface area perpendicular to the line connecting the center of the detector with the center of the total detected area. Substitution of Eq.10 into Eq.2 gives:

$$L_{meas} = \sum_{i\ ^{o}\ A_s} \frac{\rho\, r^2\, E \cos|\theta_z - \theta_{bi}|\ \ A_{si}\cos\theta_{si}\ \cos\theta_{di}}{\pi\, r_i^2 \cos\theta_d\ A_s\cos\theta_s} \qquad (11).$$

The detector area canceled, but other simplifications are only possible by assuming simple geometries. The fact that all facets within the bottom area viewed by the radiance detector must be counted is symbolized by i º A_s in the sum. We remind the reader that parameters with subscripts i refer to individual facets, whereas parameters without that subscript refer to the entire source or detector area parameters. The above expression is only valid for a collimated light field with solar zenith angle θ_z. More complex expressions using the entire light field can be written, but they do not illustrate as well how the various parameters influence the far field reflectance.

We thus conclude that the radiance measured by a finite detector depends on above water lighting conditions and the sea surface through E, the bottom morphology through all parameters with subscript i , and the detector geometry through all parameters with subscript d. When attenuation of the radiance is taken into account, the measured radiance will also depend on the IOP.

APPLICATION TO REAL SENSORS

The definition of radiance (Jerlov, 1976, Mobley, 1994) implies that both detector and source areas be vanishingly small. Real radiance detectors have finite detector areas and field of views. The Satlantic TSRB was widely used during CoBOP for the measurement of downwelling irradiance and upwelling radiance. The radiance detector has a field of view half angle of 5º. The upwelling radiance detector thus sees an area of the bottom that depends on its height above the bottom and may include many small scale topographic features. Again, we will only consider a collimated incoming radiance field. We conceptually divide the area of the bottom viewed by the radiance detector into a number of equal small areas ΔA_i. These areas are parallel to the surface . Each of these areas ΔA_i is the horizontal projection of a bottom area A_{si}, with a slope θ_{bi} ,relative to the horizontal. Radiance detectors should be designed so that their field of view, Ω_d, is small. If that is the case, the individual areas A_{si}, within the larger area viewed by the detector have very nearly the same angle θ_{di} , between the center of the detector and the center of the small areas. In Eq.11 we may then set $\cos\theta_{di}$ $\cos\ \theta_d$, so that these parameters cancel.

In the case of a TSRB at the surface the distance to the bottom is usually much larger than the bottom morphology features. In that case r_i r . If the average bottom is parallel to the sea surface, we may set $\cos\theta_s = 1$. Eq.9 then reduces to:

$$L_{TSRB} = \sum_i \frac{\rho E \cos|\theta_z - \theta_{bi}|\ A_{si}\cos\theta_{si}}{\pi A_s} \qquad (12)$$

Note that $A_{si}\cos\theta_{si} = \Delta A_i$. The small surface areas parallel to the surface add up to the total surface area viewed by the detector:

$$A_s = \sum_i A_{si}\cos\theta_{si} \qquad (13)$$

If we divide the total surface area parallel to the sea surface, A_s , into N equal areas, ΔA, where $\Delta A = A_{si}\cos\theta_{si}$, as before, we can further reduce Eq.12 to:

$$L_{TSRB} = \sum_i \frac{\rho\, E \cos|\theta_z - \theta_{bi}|}{N\pi} \quad = \frac{\rho\, E <\cos|\theta_z - \theta_b|>}{\pi} \qquad (14a)$$

The radiance detected by the TSRB thus does not depend on the angle of the sensor relative to the bottom (or surface), but does depend on the average value of the cosine of the angle of the bottom with respect to the zenith angle of the irradiance, $<\cos|\theta_z - \theta_b|>$. We remind the reader that the conclusion is only correct if the irradiance E is collimated. In the general case a more complicated expression involving Eq.3b can be written.

Since the radiance from a Lambertian source is given by $L = \rho\, E/\pi$, we see that the effective reflectance for a bottom with morphology is :

$$\rho_{eff} = \rho <\cos|\theta_z - \theta_b|> \qquad (14b)$$

It is now also clear that the effect of the IOP did not need to be considered separately for the simple geometry of collimated radiance. We can simply use ρ_{eff} in place of ρ. The effect of the IOP in radiative transfer calculations is precisely the same (provided the morphology is small enough to ignore changed path lengths), only the bottom reflectance has changed. We can thus use standard radiative transfer models, but with the adjusted reflectance.

ANALYTICAL 2-D MODEL FOR SAW TOOTH SHAPED BOTTOMS

Real bottom morphology requires numerical modeling. By using a simple geometric shape for the bottom it will be possible to derive analytical expressions for the dependence of the measured reflectance on bottom morphology and viewing angle of the detector. A reasonable approximation is the saw toothed bottom in which the bottom is piecewise linear with slopes alternately equal to θ_b and $-\theta_b$. For a saw tooth shaped bottom with amplitude A and wavelength λ, $\theta_b = \mathrm{atan}(4A/\lambda)$. This bottom has the advantage that all bottom facets have the same absolute slope relative to the horizontal. The far field reflectance (ρ_{ff}) relative to the reflectance of a flat bottom for collimated incident light with a zenith angle of θ_z and for a saw tooth shaped bottom can be obtained from Eq.12 :

$$\rho_{ff}/\rho = 0.5\cos[\theta_z + \mathrm{atan}(4A/\lambda)] + 0.5\cos[\theta_z - \mathrm{atan}(4A/\lambda)]. \qquad (15)$$

A similar expression for a sinusoidal bottom with amplitude A and wavelength λ is:

$$\rho_{ff}/\rho = (1/2\pi)\int_0^{2\pi} \cos\{\theta_z + \mathrm{atan}[(2\pi A/\lambda)\sin(2\pi x/\lambda)]\}dx \qquad (16)$$

For a saw tooth wave and zenith sun, we can thus readily calculate the effective reflectance. The average cosine of the bottom slope is simply the cosine of the saw tooth with the horizontal. An approximate angle of repose for sand is 34°, but can be much higher if the organic content is high (R. Wheatcroft, personal communication). Use of such a value is also supported by Allen (1984). We can thus approximate the ratio of the far field reflectances of a saw tooth shaped bottom at a 34º angle and a flat bottom as being cos(34) = .829. The reflectance of the saw toothed bottom is about 17% smaller. The decrease in reflectance is 23% if the bottom angle increases to 40º. If the zenith angle of the irradiance striking the bottom is 20º, Eq.15 shows that the ratio of the reflectances would be about 22% for a 34º bottom slope and 28% for a 40º bottom slope. These values give a rough indication of the range of errors to be expected, when bottom morphology is ignored. Numerical results for sinusoidal bottoms with the same amplitudes and wavelength as a saw tooth are within a few percent. Eq.15 is thus useful for estimating potential errors in a given location, if the bottom morphology is known. Note that the presence of morphology always results in lower far field reflectances and hence a "darker" looking bottom. Far field implies that the sensor sees a large number of facets. In the next section we will consider the resultant reflection when the sensor views only a limited number of bottom facets.

The number of bottom facets included in the reflectance influences the effective reflectance. Let us again consider the saw tooth bottom as a simple example that lends itself readily to analysis. If the IOP are ignored, distance from the bottom can be used to estimate the effect of including more bottom features in the field of view of the sensor. Consider incoming light irradiating the bottom from one side. Eq.14 shows that very near the bottom one would either be looking at a facet towards the incoming irradiance, or away from it. The reflectance thus would be

$\cos[\theta_z + \operatorname{atan}(4A/\lambda)]$ or $\cos[\theta_z - \operatorname{atan}(4A/\lambda)]$.

As one backed away from the bottom more and more facets would come into view, with the reflectance eventually reaching the far field value of Eq.14. The reflectance as a function of distance from the bottom would thus be an oscillatory saw tooth function. A two dimensional analysis of this can be carried out analytically for a saw tooth bottom. A 2-D saw tooth bottom in the plane of the irradiance has facets towards the sun and facets away from the sun. If the footprint of the sensor on the bottom is given by P when the sensor is a distance r above the bottom, and the wavelength of the saw tooth bottom is λ, the sensors would view $2P/\lambda$ facets. If the number of facets in view towards the sun is given by N_T and those away from the sun by N_A, then $N_T + N_A = 2P/\lambda$. The bottom reflectance will then be:

$$\rho(r)/\rho = (\lambda N_T/2P)\cos[\theta_z + \mathrm{atan}(4A/\lambda)] + (\lambda N_A/2P)\cos[\theta_z - \mathrm{atan}(4A/\lambda)]. \qquad (17)$$

At most, for any given distance from the bottom, the sensor can see one more facet of one kind than the other, hence the maximum reflectance is measured when $N_T = N_A + 1$, and the minimum when $N_A = N_T + 1$. At a distance r from the bottom, the maximum reflectance that could be observed would then be

$$[\rho(r)/\rho]_{max} = \rho_{ff}/\rho + (\lambda/4P)\cos[\theta_z + \mathrm{atan}(4A/\lambda)] - (\lambda/4P)\cos[\theta_z - \mathrm{atan}(4A/\lambda)]. \qquad (18)$$

The minimum reflectance that could be observed would be:

$$[\rho(r)/\rho]_{min} = \rho_{ff}/\rho - (\lambda/4P)\cos[\theta_z + \mathrm{atan}(4A/\lambda)] + (\lambda/4P)\cos[\theta_z - \mathrm{atan}(4A/\lambda)]. \qquad (19)$$

The maximum and minimum errors thus change proportionately to $\lambda/4P$. If the half angle of the detector is given by γ, $P = 2r \tan\gamma$, so that the maximum error is proportional to λ/r and hence the measured reflectances approach the far field reflectance for large r. The error also depends on the placement of the sensor relative to the crests and troughs of the bottom. If initially the sensor is placed at the top of the crest, and is backed away, the observed reflectance would always be the far field reflectance, because an equal proportion of facets towards and away from the irradiance would always be seen. If, however, the sensor is initially placed facing the center of a facet, as it is backed away from the bottom, the maximum and minimum reflectances as per Eqs.18 and 19 will be encountered alternatively. This phase error is proportional to the distance of the vertical projection of the center of the sensor and the center of a facet. This shows that in the near field placement of the sensor relative to the bottom morphology has a major influence on the measured reflectance. Returning to the earlier example of a 20º zenith angle for the irradiance and a 34º bottom slope, the maximum reflectance would be $\rho \cos(14) = 0.97\rho$ encountered just above the facets facing the irradiance. The minimum reflectance would be $\rho \cos(54) = 0.59\rho$ for the facets away from the incoming irradiance. As the sensor is backed away eventually the far field reflectance of 0.78ρ is reached. The amplitude of the oscillation of the reflectance as the sensors is backed away from the bottom therefore depends on the placement of the detector relative to the crest. This is also an example of the range of reflectances that may be encountered when measurements are carried out above a sand dune. A difference of up to 40% in reflectance or radiance could be measured depending on the orientation of the dune slope relative to the irradiance.

DISCUSSION AND CONCLUSIONS

We have shown that the effect of bottom morphology on the far field or effective reflectance can be substantial and cannot be ignored. We examined simple cases in which the radiance field was collimated and could be described by a single parameter, the zenith angle θ_z . Similarly we examined a simple bottom form, the saw tooth, whose slope could be described by the single angle θ_b. Depending on wavelength and amplitude this can be an approximation for both sand ripples and much larger underwater sand dunes. This resulted in the simple expression Eq.14 for the far field reflectance. We showed that for a flat sea surface and a saw tooth bottom with a slope around the angle of repose for loose sand, the far field reflectance can be approximately 20% smaller than the material reflectance. If there are organics in the bottom sediment, the angle of repose can be much larger (R. Wheatcroft, personal communication) and the far field reflectance can decrease much more. We showed that if the angle of incidence of the radiance changes away from the vertical, the far field reflectance is reduced further. In general we can thus conclude that the larger the average cosine of the light field and the larger the average slope of the bottom, the larger the deviation of the far field reflectance from the material reflectance. This would thus be a guide for where to carry out closure experiments without the influence of bottom morphology.

In the near field the reflectance depends on the horizontal and vertical placement of the sensor. This leads to the important conclusion that at least in the near field, the bottom morphology cannot be dealt with in a statistical manner. It is important whether or not the field of view of the radiance sensor primarily sees facets towards the illumination or away from it. This effect is obviously more important the larger the wavelengths of the bottom features.

In the general case the radiance is not collimated and the bottom is not simply described. The general case solution for a Lambertian bottom is obtained by substituting $E \cos|\theta_z - \theta_b|$ in Eq. 11 by $E_s(x,y,b)$ as obtained from Eq.3b. The general case is clearly much more complicated and can only be solved by means of numerical calculations. In addition, if the bottom is not Lambertian one must use the BRDF.

When dealing with shallow waters one has the additional complication of surface waves. In shallow waters with waves the light field is clearly not homogeneous horizontally and the plane parallel assumption does not hold (Zaneveld et al., 2001). This manifests itself through the light and dark patterns seen on the bottom in shallow waters (the swimming pool bottom effect). There is a non linear interaction between these patterns and the bottom. Fig.2 shows a ray diagram for a wavy surface and a sinusoidal bottom. Clearly, the radiance signal would depend on placement of the sensor relative to the surface waves with their focal points, as well as the bottom features. Eq.3b shows that one could average over time and obtain a long term average far field reflectance. The non-linearity of the problem shows that one cannot simply separate the average characteristics of the light field and the average characteristics of the bottom. Analysis of the general case by means of numerical models will be the subject of future study.

In this paper we have ignored the effects of absorption and scattering. The reflectance or BRDF of a bottom does not involve the IOP of the water column. It thus was of interest to derive an equivalent expression for the far field reflectance of a bottom with morphology. This was possible only for parallel radiance. Light scattering redirects radiance. Eq.3b shows that light scattering which is symmetric about the original direction will result in decreased radiance reflected from the bottom. On the other hand, light absorption tends to decrease the zenith angle of the radiance. This can increase or decrease the reflected radiance depending on $|\theta_z - \theta_b|$.

A closure experiment was carried out during the CoBOP experiment at the Rainbow South site. This site is 2-3m deep and was characterized by a sand bottom with large scale features. This is thus a case where even at the surface the far field reflectance does not apply and the measured reflectance or radiance is a function of placement of the sensor relative to the bottom features and their placement relative to the irradiance. The total scattering coefficient at 440 nm measured at this site was between 0.14 and 0.25 m^{-1}. The bottom is thus well within one scattering depth of the surface. The range of the total absorption coefficient was 0.045 to 0.115 m^{-1}. The absorption depth was thus larger than 9m. Consequently at that wavelength little scattering and absorption modified the radiance impinging on the bottom, so that results in this paper would apply with little error. The same would be true in the red, where the measured total scattering coefficient was less than in the blue. The total absorption coefficient at 660 nm was 0.35 to 0.37 m^{-1}.

There would thus be some redirection of the radiance to the vertical. The influence of this on measured radiance would depend on the bottom slope and orientation.

ACKNOWLEDGMENTS

This work was supported by the Environmental Optics program of the Office of Naval Research as part of the Coastal Benthic Optical Properties program. We wish to thank Dr. W. Philpot for insightful discussions.

FIGURE CAPTIONS

Figure 1. The definition of radiance.

Figure 2. The non-linearity of the interaction of the light field and the bottom. Shown is a ray diagram for parallel light at an angle of 10º to the vertical above the sea surface, a surface wave of wavelength 1m and amplitude of 0.04m, a bottom wave of wavelength 0.4m and amplitude of 0.1m, and a radiance detector with a half angle of 3º located 0.7 m beneath the sea surface. Horizontal and vertical scales are different.

REFERENCES

Allen, J. R. L.. 1982. Sedimentary structures. Vol. 1. Elsevier.

Mobley, C.D. 1984. *Light and Water,* Academic Press.

Jerlov, N.G. 1976. *Marine Optics,* Elsevier.

Voss, K.J., A. Chapin, M. Monti and H. Zhang. 2000. Instrument to measure the bidirectional reflectance distribution function, Applied Optics, **39**, 6197-6206.

Wheatcroft, R.A.. 1994. Temporal variation in bed form configuration and one-dimensional bottom roughness at the mid-shelf STRESS site. Cont. Shelf Res. **14**, 1167-1190.

Zaneveld, J.R.V., E. Boss, and A. Barnard. 2001. Influence of surface waves on measured and modeled irradiance profiles. Applied Optics, **40**, 1442-1449,

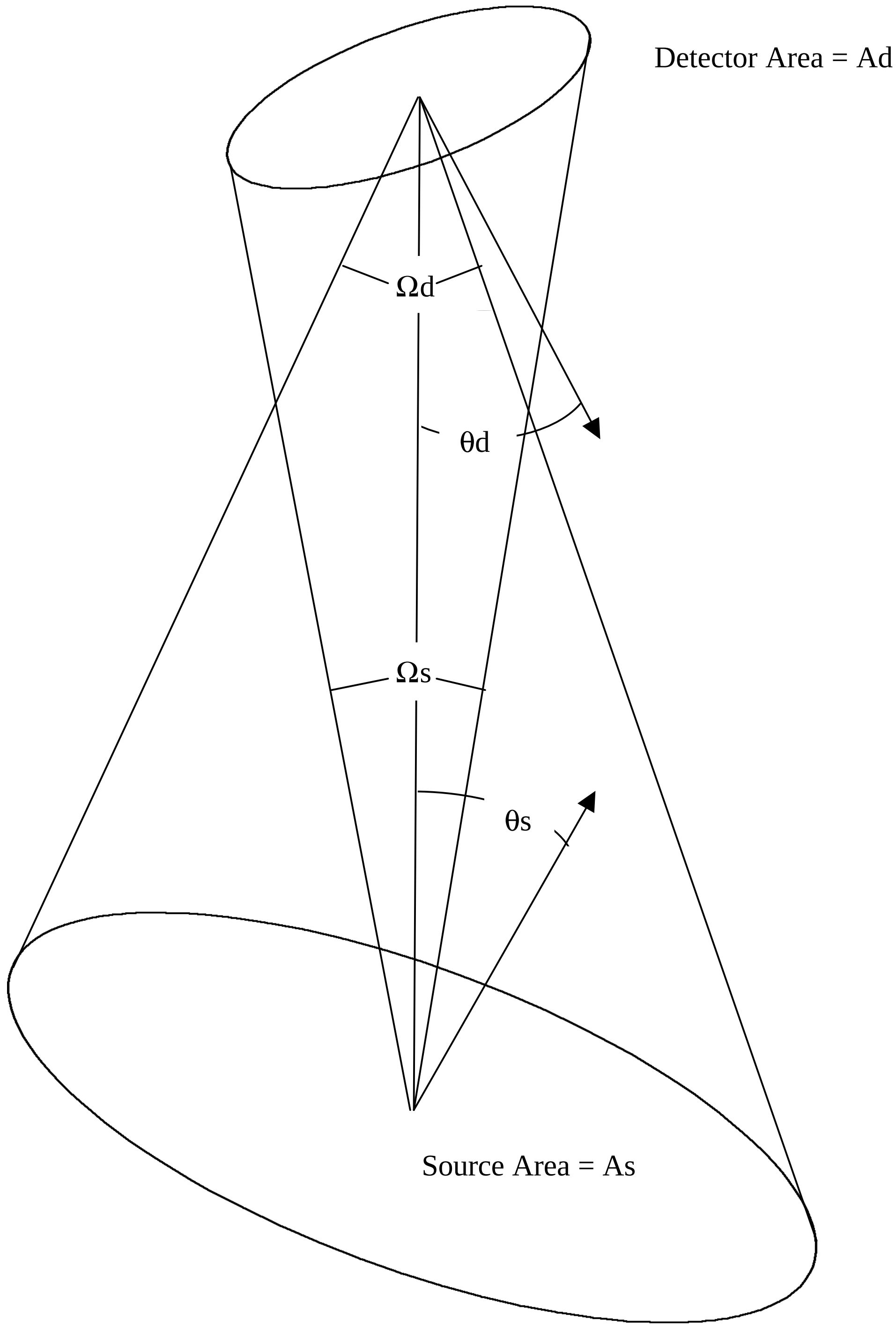
Detector Area = Ad
Ωd
θd
Ωs
θs
Source Area = As

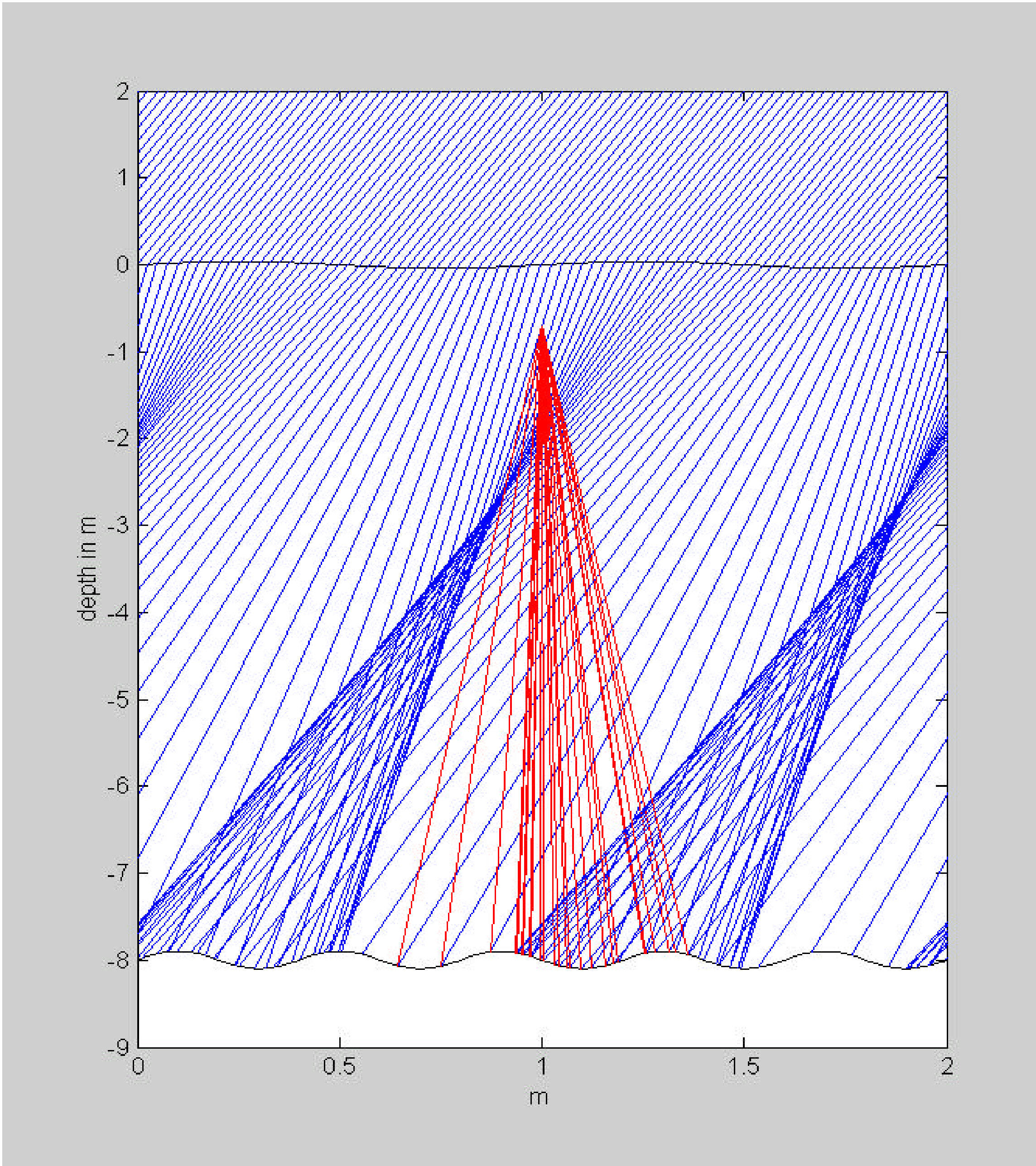

Fig.2